Large-Scale Background and the Role of Quasi-Biweekly Moisture Transport in the Extreme Yangtze River Rainfall in Summer 2020

Yanjun Qi (qiyj@cma.gov.cn)
Chinese Academy of Meteorological Sciences https://orcid.org/0000-0003-3072-2891
Renhe Zhang
Department of Atmospheric and Oceanic Sciences
Zhuo Wang
University of Illinois at Urbana-Champaign Department of Atmospheric Sciences

Research Article

Keywords: quasi-biweekly oscillation, large-scale circulation, moisture transport, extreme Yangtze River rainfall

Posted Date: January 10th, 2022

DOI: https://doi.org/10.21203/rs.3.rs-885094/v1

Large-scale background and the role of quasi-biweekly moisture transport in the extreme Yangtze River rainfall in summer 2020

Yanjun Qi[1], Renhe Zhang[2] and Zhuo Wang[3]

1 State Key Laboratory of Severe Weather, Chinese Academy of Meteorological Sciences, Beijing, China
2 Department of Atmospheric and Oceanic Sciences and Institute of Atmospheric Sciences, Fudan University, Shanghai, China
3 Department of Atmospheric Sciences, University of Illinois at Urbana Champaign, Illinois, USA

Corresponding author:
Yanjun Qi, Chinese Academy of Meteorological Sciences, Beijing, China.
Email: qiyj@cma.gov.cn

Abstract

A severe flooding hit southern China along the Yangtze River in summer 2020. The floods were induced by heavy rains, and the associated dynamic and thermodynamic conditions are investigated using daily gridded rainfall data of China and NCEP-NCAR reanalysis. It is found that the summer rainfall over the Yangtze River Basin (YRB) experienced pronounced subseasonal variation in 2020, dominated by a quasi-biweekly oscillation (QBWO) mode. The southwestward-moving anomalous QBWO circulation was essentially the fluctuation of cold air mass related to the tropospheric polar vortex or trough-ridge activities over the mid-high latitude Eurasian in boreal summer. The large-scale southwestward-transport of cold air mass from mid-high latitudes and the northeastward-transport of warm and moist air by the strong anomalous anticyclone over the western North Pacific provided important circulation support for the heavy rainfall in the YRB. The quasi-biweekly anomalies of potential and divergent component of vertically integrated water vapor flux played a major role in maintaining the moisture during summer 2020. The diagnosis of moisture budget shows that the enhanced moisture associated with the quasi-biweekly fluctuation rainfall was primarily attributed to the moisture convergence. The convergence of QBWO specific humidity by the background mean flow and convergence of mean specific humidity by QBWO flow played dominant roles in contributing to the positive moisture tendency. In combination with an adiabatic ascent induced by the warm temperature advection, the boundary layer moisture convergence strengthens the upward transport of moisture from lower troposphere. The vertical moisture transport associated with boundary layer convergence was of critical importance in causing low-level tropospheric moistening, whereas the horizontal advection of moisture showed a negative effect during the anomalous quasi-biweekly summer rainfall in 2020.

Keywords: quasi-biweekly oscillation, large-scale circulation, moisture transport, extreme Yangtze River rainfall

1. Introduction

In summer 2020, record-breaking severe floods hit southern China from the middle to lower reaches of the Yangtze River valley. The floods were induced by heavy rains from June to August and affected 54.8 million people in 27 province. About 368,000 houses were destroyed, and direct economic losses amounted to 144.43 billion yuan (20.66 billion US dollars) by 29 July 2020 (http://www.xinhuanet.com/english/2020-07/29/c_139247689.htm). Some of towns in the central and southern provinces received record-breaking precipitation in June and July (https://mp.weixin.qq.com/s/SScXrBYG2TJfLKc0BmIp2Q). In the continuous heavy rainfall periods, eastern China, especially the lower Yangtze River Basin, suffered flooding and severe damage after multiple rainstorms. The accumulative rainfall during summer 2020 set the highest record since 1961. The floods were reminiscent of the 1998 China floods that caused life and economic losses. In fact, the summer floods in 2020 were actually more impactful as the floods hit the populated regions not only in eastern China but also in southern Japan.

The interannual variability of East Asian summer monsoon is characterized by rainfall anomalies from the middle-lower reaches of the Yangtze River in China to southern Japan. A series of studies have investigated the record-breaking summer rainfall in 2020 using numerical model simulations or/and observations. Although operational forecast models successfully captured the enhanced rainfall in the Yangtze River Basin (YRB) in summer 2020, the magnitude of rainfall anomalous was underestimated (Li et al., 2021a). The factors responsible for the extreme rainfall were associated with the large-scale atmospheric circulation anomalies related to tropical and extratropical forcing. Zhou et al. (2021) proposed that the slowly westward propagation of oceanic Rossby waves in the South Indian Ocean induced by a strong Indian Ocean Dipole event in the late 2019 was the key process. The oceanic Rossby waves help sustain the Indian Ocean warming and intensify the anomalous anticyclone over the western North Pacific (WNP) through the Indo-western Pacific Ocean capacitor mechanism (Xie et al., 2009), and further leads to the extreme rainfall in the YRB in summer 2020. A similar conclusion was reached through climate model simulations using the coupled seasonal prediction system of Japan Meteorological Agency (Takaya et al., 2020). Pan et al. (2021) further demonstrated that the extremely strong anomalous anticyclone over the WNP resulted from a combined effect of a quick El Niño to La Niña phase transition besides the effect of strong Indian Ocean warming. In addition to the tropical Indo-Pacific large-scale thermal condition, the positive sea surface temperature anomalies in the Atlantic Ocean contributed to the extreme rainfall through an atmospheric wave train across Europe, including an anomalous anticyclone over the WNP (Wang 2019; Zheng et al., 2021). Zhang et al. (2021) emphasized the important role of the Madden-Julian Oscillation (MJO), with an extraordinary long-lasting and quasi-stationary active phase over the Indian Ocean during June-July 2020, contributing to the heavy rainfall (Liang et al., 2021). Li et al. (2021b) illustrated that the eastward moving vortices from Tibetan Plateau may trigger the heavy Meiyu rainfall in summer 2020. Ding et al. (2021) pointed out that the evolution and configuration of the East Asian summer monsoon circulation subsystems, including quasi-biweekly oscillation (QBWO) of the western North Pacific subtropical high, the blocking highs and troughs in middle- high latitude Eurasia, the upper-level westerly jet, and low-level southwesterly flow, played an important role in triggering and maintaining the excessive and persistent rainfall along the YRB.

Statistical analysis shows that the summer rainfall in the Yangtze River basin exhibits not only interannual variability but also intraseasonal variability (Mao et al., 2006, 2010; Hsu et al., 2016; Qi et al., 2019; Yan et al., 2019; Liu et al., 2020b; Ding et al., 2020). The subseasonal perspective of the record-long 2020 summer rainfall was examined by Qiao et al. (2021), who suggested that subseasonal variations of the long-lasting floods were modulated by the tropical and extratropical teleconnections. The extreme rains can be attributed to different systems at the different stages, including the East Atlantic/West Russia teleconnection, the Pacific-Japan pattern, and the combined effect of tropical forcing and mid-latitude teleconnection. The purpose of this study is to investigate the subseasonal variations of dynamic and thermodynamic conditions contributing to the extreme rains and floods in summer 2020. We will mainly focus on the role of moisture transport in the occurrence and maintenance of heavy rainfall, and the scale interactions between the background mean state and subseasonal variability of the moisture convergence and advection to examine the relative contributions among the decomposed component terms to the excessive rainfall along the Yangtze River basin in summer 2020.

Data and analysis methods are introduced in section 2. The quasi-biweekly rainfall fluctuation in summer 2020 and the associated large-scale moisture transport are described in section 3. In section 4, we discuss the contributions of the moisture convergence and advection to extreme rainfall using the moisture budget analysis. Conclusions and discussions are given in section 5.

2. Data and Method

The daily gridded rainfall data with a resolution of 0.5° × 0.5°from the National Meteorological Information Center of China Meteorological Administration are used to depict the spatial distribution and subseasonal variations of rainfall in eastern China in summer 2020. This dataset is based on the daily rain gauge measurements over 2400 stations in the Chinese national dense observational network (Shen and Xiong, 2016). The National Center for Environmental Prediction-National Center for Atmospheric Research (NCEP-NCAR) reanalysis at a 2.5° × 2.5° spatial resolution (Kalnay et al., 1996) is utilized. Daily mean winds, pressure vertical velocity, geopotential height, air temperature and specific humidity on standard pressure levels are used to analyze large-scale atmospheric circulation and diagnose moisture budget associated with extreme rainfall.

The wavelet spectrum analysis (Torrence and Compo, 1998) is used to extract the dominant signal of summer rainfall in 2020 over the YRB. Before performing the wavelet analysis, the annual cycle and its first three Fourier harmonics are removed from the daily mean rainfall. To isolate subseasonal signals, daily rainfall and other atmospheric variables including zonal and meridional winds, vertical velocity, geopotential height, specific humidity, and temperature at each standard pressure level are subjected to a 10-20-day bandpass filtering based on the harmonic decomposition

(Kemball-Cook et al., 2002; Teng and Wang, 2003; Jiang et al., 2004; Qi et al., 2008).

The total water vapor flux $\mathbf{Q}$ can be written as

$$\mathbf{Q} = \frac{1}{g}\boldsymbol{V}q \qquad (1)$$

where g is the gravity, wind vector $\boldsymbol{V} = u\hat{\imath} + v\hat{\jmath}$, q is the specific humidity. Following Rosen et al. (1979), Salstein et al. (1980) and Chen (1985), the water vapor transport is decomposed into the contribution by the non-divergent and irrotational wind components based on the Helmholtz flow decomposition,

$$\mathbf{Q} = \mathbf{Q}_\psi + \mathbf{Q}_\chi \qquad (2)$$

$$\mathbf{Q}_\psi = k \times \nabla\psi, \text{ and } \mathbf{Q}_\chi = \nabla\chi \qquad (3)$$

where $\mathbf{Q}_\psi$ and $\mathbf{Q}_\chi$ denote the non-divergent and irrotational (divergent) components of water vapor flux, respectively. ψ and χ satisfy the following equations, respectively,

$$\nabla^2\psi = k \cdot \nabla \times \mathbf{Q}, \text{ and } \nabla^2\chi = \nabla\cdot\mathbf{Q} \qquad (4)$$

The above equations are used to display the relationship between the large-scale atmospheric circulation and water vapor transport.

The decomposition of the quasi-biweekly perturbation and the low-frequency background state associated with moisture budget is described in section 4.

3. Quasi-biweekly fluctuation of extreme summer rainfall and moisture transport

3.1 Features of summer rainfall and associated atmospheric circulation

In the summer of 2020, the central-southern part of China was hit by the heavy rainfall as shown in Fig. 1a. The regions around the north and the south of middle to lower reaches along the Yangtze River in Hubei, Anhui, Jiangsu and Zhejiang provinces were hit by floods with a historical record since 1998. Some of these areas experienced strong rainstorms with the maximum precipitation more than 1200 mm during June-August (JJA). The anomalous JJA rainfall in 2020 departed from climatology shows pronounced positive rainfall anomalies along the Yangtze River basin from upper to lower reaches (Fig.1b). The maximum precipitation center was located over the eastern part along the River, which led to floods over there.

Figure 2 displays time-latitude section of daily rainfall in eastern China from May to August. Previous studies (e.g. Lau et al., 1988) showed that the prominent feature of the major rainband over eastern China appears to evolve northward progression from south to north in climatology mean. The subseasonal northward movement of summer rain belt exhibited the similar behavior in 2020 compared with the climatology, but the intensity and duration of Meiyu front rainfall were different from previous years (Qi et al., 2016). The Meiyu front develops in mid-May in the southern China and the rain belt shifted northward to the Yangtze River basin around 30°N in early June, persisting until late July with a couple of short break periods. The disastrous floods along the YRB can be attributed to both the intensity and duration of the enhanced rainfall. The rain belt then shifted poleward in early August associated with the northward advance and southward retreat of the subtropical high over the WNP (Tao et al., 2006).

The large-scale atmosphere circulation associated with the extreme strong rainfall developed meridionally and transported the cold air southeastward from the mid-high latitudes to eastern China. The500 hPa geopotential height field shows an anomalous low over the sea of Okhotsk during June-August of 2020 (Fig. 3b). It has a barotropic structure and is associated with a low-level anomalous cyclonic circulation, including an anomalous northeasterly flow along the coast. The anomalous cyclonic vorticity accompanied by the cold air in the northeastern Asian provided the favorable environmental conditions for the strong precipitation in the YRB. Meanwhile, an unusually strong subtropical high in the WNP extended further westward to the southern China in 2020 compared with the climatological mean (Fig. 3a). The southwesterlies in the northwest flank of subtropical high transported the warm and moist air from the tropics toward the Yangtze basin and converged with the northeasterlies, yielding an anomalous convergence zone along the Yangtze River and leading to the increase of rainfall. The distribution of meridional shear vorticity at 850 hPa with positive vorticity anomaly along Yangtze River and negative anomaly over southern China, which was first proposed by Wang and Fan (1999) in defining a shear vorticity index to measure the East Asian summer monsoon, provided the dynamic conditions for enhancing the rainfall in the Yangtze basin (Fig. 3b). This configuration of the middle and lower tropospheric circulations favored the occurrence of rainfall over the YRB. The anomalously strong western Pacific subtropical high played a critical role in enhancing rainfall over the Yangtze River basin.

3.2 Quasi-biweekly fluctuations

The daily rainfall in Fig. 2 is characterized by strong subseasonal variability. Strong subseasonal variations of summer rainfall in 2020 occurred in the middle to lower reaches of the Yangtze River (Fig. 4), collocated with large climatological mean rainfall (Qi et al., 2019). The Yangtze River basin, which is highlighted by a box (114°-118°E, 28.5°-32.5°N) in Fig. 4, is subject to severe floods frequently in summer, such as the extreme floods in 1991 and 1998 (Mao et al., 2006; Qi et al., 2016).

To investigate the dominant signal of the subseasonal variability in summer rainfall in 2020, the wavelet analysis (Torrence and Compo, 1998) is applied to daily rainfall in the key region (indicated by the box in Fig.4) in 2020, with the first four harmonics removed. Figure 5 displays the normalized wavelet power spectrum for the time series of areal mean rainfall in the key region. It is noted that a significant quasi-biweekly mode with the period 10-20 days during June-August 2020. The result is consistent with Ding et al. (2021) who presented that the quasi-biweekly oscillation (QBWO) was associated with the onset, northward shift, and retreat of the rain belt during the Meiyu season of 2020.

The time series of summer rainfall in 2020 over the key region is applied to the 10-20-day bandpass filtering based on the harmonic decomposition. It is shown that the rainfall anomalies in the YRB exhibited several remarkable 10-20-day cycles from June to August (Fig. 6). These filtered cycles corresponded well with the rainfall anomalies. The peak wet and dry phases represent the maximum positive and negative rainfall anomalies in the cycles, respectively. Three cycles with the amplitude exceeding one standard deviation of 10-20-day filtered rainfall anomalies were selected for composite analysis of wet and dry phase. The peak wet and dry phases are marked with solid black triangles in Fig. 6.

To reveal the impacts of large-scale atmosphere circulation from the mid-high latitudes on the QBWO of rainfall in the YRB, we constructed lead/lag composites of the 10-20-day filtered geopotential height and horizontal winds based on the selected three strong QBWO cycles. Day 0 corresponds to the maximum positive rainfall anomaly, or the peak of the QBWO wet phase. The time sequence of the composite from day -8 to 6 (with a 2-day interval) in 10-20-day filtered geopotential height and winds anomalies at 200 hPa is illustrated in Fig. 7. At day -8, a strong positive height anomaly accompanied by an anomalous anticyclonic circulation appeared to the Central Siberian plateau and a negative height anomaly was on the eastern side of the plateau. In the ensuing days, the positive height anomalies and the corresponding anticyclonic circulation weakened and expanded westward and southward, while the negative height anomaly and corresponding cyclonic circulation intensified as it moved southwestward. At day 0, an anomalous cyclone extends from east of the Urals to the Sea of Okhotsk with the center over the Lake Baikal. After that, it began to weaken as continuing to move westward (Fig. 7). This westward propagating QBWO geopotential height anomaly was part of the westward circulation of polar vortex with a clockwise rotation in the eastern hemisphere in boreal summer (Yang et al., 2013). The southwestward-moving quasi-biweekly oscillation anomalous circulation was essentially the fluctuation of cold air mass which was closely related to the polar vortex or trough-ridge system activities over the Eurasian mid-high latitudes in boreal summer. The vertical distribution of the QBWO geopotential height anomaly evolution had a barotropic structure (Figures not shown), suggesting that the strong cold air affecting the extreme summer rainfall in eastern China in 2020 originated from the polar vortex.

3.3 Water vapor transport and maintenance

The relationship between the atmospheric circulation and the water vapor transport can be illustrated by means of the streamfunction and potential (Chen, 1985). Figure 8 shows the streamfunction with non-divergent field and potential with irrotational (divergent) field of the vertically integrated (1000-300 hPa) water vapor flux in June-August of 2020. The spatial pattern and intensity of large-scale water vapor transport can be delineated by the streamfunction and nondivergent component as shown in Fig. 8a. It exhibited a three-cell structure in the Northern Hemisphere and a two-cell in the Southern Hemisphere. Each cell corresponds to an anticyclonic transport of water vapor in the oceans or monsoon region. The zonal characteristics of the nondivergent field indicated a strong westward transport of water vapor in the tropics and strong eastward transport in the mid-latitude of both hemispheres. During June-August in 2020, the strong three cells of anticyclonic transport in the Northern Hemisphere were centered over the Pacific, Atlantic and equatorial Indian Ocean to South Asian monsoon region, respectively. The intensity of the Pacific Ocean cell was strongest, possibly due to the intensification of the water vapor transported by the low-level tropical circulation over the Pacific Ocean. As shown in Fig. 8a, there were two sources of water vapor transport that led to the heavy rainfall in the YRB. One is the northeastward water vapor transport from the Indian Ocean. Noted that this transport originated from the westward transport of easterly in the south of equator and turned to eastward when it reached the east coast of Africa. Another transport pathway was the northward transport associated with the anticyclonic circulation over the South China Sea (Fig. 8a).

Figure 8b shows the potential and divergent component of vertically integrated water vapor flux that described the maintenance of moisture during the period of heavy rainfall. The strongest convergence of water vapor flux appeared over the Southeast Asia in June-August of 2020. The convergence of water vapor flux tends to contribute to an increase in column water vapor. When combined with upward motion, it tends to enhance condensation and precipitation. The large-scale moisture convergence is thus an important moisture supply for the extreme rainfall in 2020. Although the magnitude of potential was smaller than that of streamfunction, the divergent component of the water vapor flux plays an important role in the water vapor budget. Both the water vapor transport and convergence of water vapor flux in the YRB in summer 2020 were much stronger than the climatological mean compared with the statistical result (Qi et al., 2019).

To investigate the quasi-biweekly fluctuation in the large-scale transport and convergence of water vapor flux, the 10-20-day filtered streamfunction and potential of the vertically integrated water vapor flux is presented in Fig. 9. The pattern of the QBWO anomalous streamfunction and potential was similar to that in the summer mean in the East Asian monsoon region, suggesting that the QBWO was the dominant mode in the water vapor flux associated with the summer rainfall. The positive streamfunction anomalies associated with anticyclonic water vapor transport were still located over the western North Pacific and Indochina monsoon region as the summer mean. The strong anomalous westerlies transported the positive moisture anomalies toward the YRB and southern Japan during the peak wet phase (Fig. 9a). A strong convergence anomaly of the water vapor flux dominated the East Asian summer monsoon region with the center in the equatorial maritime continent east of the Philippines (Fig. 9b). It indicates that a large amount of moisture transported from the WNP and South Asia monsoon region was converged toward the YRB to enhance the moisture supply for the heavy rainfall during the peak wet phase. The quasi-biweekly anomalies of the potential and divergent component of water vapor flux played a critical role in maintaining the Meiyu rainfall fluctuations during June-August in 2020.

The vertical structures in vertical motion, specific humidity and wind divergence further illustrate the thermal and dynamic conditions contributing to heavy rains. Figure 10 displays the vertical structures of 10-20-day filtered specific humidity and vertical motion between 110°E and 120°E for the peak dry and peak wet phase. In the peak dry phase, the YRB was characterized by the subsidence associated with low-level divergence, negative vorticity, and negative specific humidity anomalies (Fig. 10a, 11a), which are not conductive to precipitation over the YRB. In contrast, during the peak wet phase, the ascending motions associated with the strong low-level convergence and upper-level divergence transport moisture upward from the boundary layer and enhance the water vapor content in the middle troposphere. The cyclonic vorticity and boundary layer moisture convergence strengthen the rainfall in the Yangtze basin (Fig. 10b, 11b).

4. Contributions of the moisture convergence and advection to the extreme rainfall

To assess the moisture tendency associated with the heavy rainfall in summer 2020, moisture budget was analyzed. According to Yanai et al. (1973), the moisture tendency at each constant pressure level is determined by the sum of horizontal and vertical moisture advections and the atmospheric apparent moisture sink Q_2 as shown in Eq. (1):

$$\frac{\partial q}{\partial t} = -V \cdot \nabla q - \omega \frac{\partial q}{\partial p} - \frac{Q_2}{L} \qquad (1)$$

where q is the specific humidity, t is the time, V is the horizontal wind vector, ∇ is the horizontal gradient operator, ω is the vertical pressure velocity, p is the pressure, Q_2 is the atmospheric apparent moisture sink, and L is the latent heat of condensation. The vertical advection term may be further decompose into the horizontal moisture convergence term ($-q\nabla \cdot \mathrm{V}$) and the vertical flux term ($-\partial\omega q/\partial p$).

Based on diagnosis of the above moisture budget, Maloney (2009), Hsu et al. (2012) and Zhao et al. (2013) analyzed the atmospheric moisture dynamic in relation to the MJO initiation, development and propagation processes. To explore the effect of moisture transport on the quasi-biweekly fluctuated rainfall in summer 2020, we applied a QBWO-filtering operator (denoted by a prime) to the above moisture tendency Eq. (1). The anomalous moisture budget equation may be derived as follows:

$$\frac{\partial q'}{\partial t} = -(\mathrm{V} \cdot \nabla q)' - (q\nabla \cdot \mathrm{V})' - \frac{\partial(\omega q)'}{\partial p} - \frac{Q_2'}{L} \qquad (2)$$

The first term in the right-hand side in Eq. (2) represents the horizontal advection of moisture, the second term the horizontal convergence of moisture, the third term the flux form of vertical moisture advection, and the fourth term moisture loss (gain) due to the condensational heating (raindrop-induced evaporation in the unsaturated atmosphere and surface evaporation) process. The combination of the second and third term represents the vertical moisture advection (Hsu et al., 2012).

To illustrate the role of quasi-biweekly perturbation in enhancing and maintaining the moisture during the period of extreme rainfall over the region of YRB, both specific humidity and winds fields are decomposed into two components:

$$q = \bar{q} + q', u = \bar{u} + u', v = \bar{v} + v' \qquad (3)$$

where an overbar and a prime denote the low-frequency background state (LFBS, with a period longer than 20 days) and QBWO component, respectively. The decomposed LFBS component includes an annual and semi-annual cycles, and seasonal to subseasonal mean state with the period longer than 20 days. The QBWO component is referred to 10-20-day perturbation, the component of synoptic time-scale less than 10 days is ignored. In order to examine the contributions to the QBWO moisture tendency by the low-frequency background state, the horizontal moisture convergence and moisture advection in Eq. (2) can be written as:

$$-q\nabla \cdot V \approx (-\bar{q}\nabla \cdot V') + (-q'\nabla \cdot \overline{V}) + (-q'\nabla \cdot V') \qquad (4),$$

and

$$-V \cdot \nabla q \approx (-\overline{V} \cdot \nabla q') + (-V' \cdot \nabla \bar{q}) + (-V' \cdot \nabla q') \qquad (5)$$

By applying a 20-day low-pass filter and a 10-20-day band-pass filter to each variable in equations (4) and (5), respectively, one may extract the LFBS and QBWO signals from the raw data.

The vertically integrated moisture convergence and advection are calculated quantitatively to show the contributions of interaction between the LFBS and QBWO perturbation to the moisture budget related to the extreme rainfall in summer 2020. Figure 12 presents the budget difference of vertical integral (from 1000 to 300 hPa) of moisture convergence and moisture advection between the peak wet and peak dry phase in three individual terms in equations (4) and (5) over the YRB. In the decomposed component of moisture convergence, all the three terms had positive contributions (Fig. 12a). The leading term $(-q'\nabla \cdot \overline{V})$, which denotes the convergence of QBWO moisture by the LFBS background mean flow, was dominant in the peak wet phase. The spatial distributions of the mean flows and QBWO specific humidity in association with $(-q'\nabla \cdot \overline{V})$ is illustrated in Figure 13a. Both mean flows and anomalous specific humidity were derived based on the peak wet phase composite and vertical integration from 1000 to 700 hPa. The maximum positive specific humidity anomaly was located in the WNP where the water vapor transport was also strongest. The mean flow was dominated by strong southerlies in the south east China. The strong boundary layer moisture convergence played a major role in moistening over the YRB. The second leading term in the moisture convergence is $(-\bar{q}\nabla \cdot \mathrm{V}')$, which was associated with the mean moisture convergence by the QBWO flow (Fig. 13b). It is found that an anomalous cyclonic circulation converged the boundary layer high moisture and transported moisture with the ascending motions upward to moisten the middle troposphere (Figs. 10, 11). The eddy-eddy term $(-q'\nabla \cdot \mathrm{V}')$, the QBWO convergence of the anomalous moisture, played a minor but positive role in moistening over the YRB (Fig. 12a).

It is worth noting that the horizontal moisture advection in terms $(-\overline{\mathrm{V}} \cdot \nabla \mathrm{q}')$ and $(-\mathrm{V}' \cdot \nabla \bar{q})$, which representing the interactions between LFBS and QBWO fluctuation, produced a negative moisture tendency. Although the quasi-biweekly eddy-eddy interaction $(-\mathrm{V}' \cdot \nabla \mathrm{q}')$ produced a positive moisture advection (Fig. 12b), the total contributions of moisture advection were negative. Noted that the magnitude in moisture advection terms were 10^4 times smaller than in the moisture convergence terms. Thus, the contributions of moisture advection with the LFBS-QBWO interactions did not contribute to the moisture positive tendency for the 2020 summer rainfall. Such feature is very different from that in the climatological mean (Qi et al., 2019). The result implies that the moisture convergence played the critical role in increasing the moisture content and in turn in generating the quasi-biweekly fluctuation rainfall over the YRB in June-August 2020.

Figure 14 shows the composite vertical profiles in 10-20-day filtered temperature advection, vertical velocity, wind divergence and specific humidity over the YRB for the peak wet and peak dry phases. The positive (negative) anomaly of temperature advection increased (reduced) with height, resulting in the ascending (descending) motion during the peak wet (dry) phase (Fig. 14a, b). The boundary layer moisture convergence contributes to the upward moisture transport to the middle troposphere because of the large-scale ascending motion adiabatically induced by the warm temperature advection during the peak wet phase over the YRB (Fig. 14c, d).

5. Conclusions and Discussions

In summer 2020, the severe flooding in decades hit southern China from the middle to lower reaches of the Yangtze River valley. The subseasonal variations of the extreme rainfall and the associated large-scale circulations related to moisture transport during summer 2020 are investigated. The maximum rainfall variability during summer 2020 appeared in the middle and lower reaches of Yangtze River basin, where dominated by a significant quasi-biweekly oscillation (QBWO) mode in the June-August rainfall. It is found that the southwestward-moving anomalous quasi-biweekly circulation was essentially the fluctuation of cold air mass which is closely related to the polar vortex or trough-ridge system activities over the Eurasian mid-high latitudes in boreal summer. In the low latitude, the western North Pacific subtropical high was strong and extended further westward in June- August 2020 compared with the climatological mean. The warm and high moisture atmosphere transported by the southwesterlies associated with the anomalous strong anticyclone in the western North Pacific converged with the cold air from mid-high latitudes over the YRB. The strong water vapor transported to the YRB came from the westward zonal transport in the equatorial Pacific Ocean and eastward zonal transport in the latitudes of the Bay of Bengal and Indo-China. The large amount of moisture was converged toward the YRB to provide moisture supply for the heavy rainfall. The quasi-biweekly anomalies of the potential and divergent component of water vapor flux played a critical role in maintaining the extreme rainfall in June-August 2020.

The diagnosis of moisture flux budget indicates that the moisture convergence played a dominant role in determining the summer rainfall in 2020. The largest contribution to the moisture convergence during the peak wet phase was the decomposed term $(-q'\nabla \cdot \overline{\mathrm{V}})$, which denotes the convergence of QBWO moisture by the background mean flow. The positive quasi-biweekly specific humidity anomaly was converged toward the YRB by the strong seasonal mean southerlies. The second leading term in the moisture convergence $(-\bar{q}\nabla \cdot \mathrm{V}')$, the mean moisture convergence by the QBWO flow, was associated with the boundary layer moisture convergence to help low-level tropospheric moisture to penetrate into the middle troposphere. With scale interactions between LFBS and QBWO in the horizontal moisture advection processes, the decomposed terms $(-\overline{V} \cdot \nabla q')$ and $(-V' \cdot \nabla \bar{q})$ produced negative contribution to the moisture. The magnitude of moisture advection terms was 10^4 times smaller than those terms of moisture convergence. It suggests that the moisture contribution to the quasi-biweekly fluctuation rainfall was primarily attributed to the moisture convergence. The boundary layer moisture convergence intensified the air moisture upward with the ascending motion which induced by the warm temperature advection. The vertical moisture advection associated with boundary layer convergence showed significant contributions to the anomalous quasi-biweekly rainfall, in addition to the favorable large-scale circulations in the tropics and mid-high latitudes which provided the essential dynamic and thermodynamic conditions for the extreme rainfall over the Yangtze River basin in June-August 2020.

As one of the important large-scale circulation factors, the anomalous anticyclone over the WNP links closely East Asian climate variations with central-eastern Pacific sea surface temperature (SST) anomalies (Zhang et al., 2017; Li et al., 2017). The anomalous anticyclone strengthens the summer Meiyu/Baiu rainfall through the northward transport of high moisture from the tropics by anomalous southerlies in the western flank of the anomalous anticyclone (Zhang, 2001). According to the previous studies, the dominant anomalous anticyclone is primarily due to the warm SST anomalies in the tropical eastern Pacific associated with El Niño event (Zhang et al., 1996, 1999; Wang et al., 2000), Indian Ocean basin-wide warming mode effect (Xie et al., 2009; Wu et al., 2009) and the warming in the tropical north Atlantic Ocean (Rong et al., 2011). The pronounced anomalous anticyclone in the WNP, which closely related to the severe floods along the Yangtze River during the summer of 2020, was not caused directly by the weak El Niño in the Pacific, but by the basin-wide warming in the Indian Ocean induced by the strong Indian Ocean Dipole event in 2019 (Zhou et al., 2021; Takaya et al., 2021) and positive SST anomalies in May over the North Atlantic Ocean (Zheng and Wang, 2021). What is the relative role of tropical boreal summer intraseasonal oscillation (BSISO) in the formation and maintenance of the strong anticyclone over the WNP? Whether are there interactions between the tropical BSISO and the QBWO circulation from mid-high latitudes? The structural evolution of BSISO related to the anticyclonic circulation and the extreme rainfall need to be further examined, and the possible impacts of the local SST and Indo- Pacific SST anomalies on the BSISO activities also need to be investigated in the future. In addition, the other interannual variabilities, such as East Asian/Pacific pattern (EAP), Silk Road pattern, North Atlantic Oscillation (NAO), and western North Pacific High, are all related to the 2020 extreme Meiyu (Ding et al., 2021; Liu et al., 2020). How importance of these climate factors in controlling the subseasonal components is also worthy of further investigation.

Acknowledgements

Constructive comments from the anonymous reviewers are greatly appreciated. This work is supported by the National Natural Science Foundation of China (41675068) and Basic Research Fund of CAMS (2021Z004 and 2021KJ030).

References

Chen T.-C., 1985. Global water vapor flux and maintenance during FGGE, Mon. Wea. Rev., 113, 1801-1819.

Ding Y. and Hu, G., 2003. A study on water vapor budget over China during the 1998 severe flood period (in Chinese). Acta Meteorologica Sinica, 61, 129-145.

Ding Y., Liang, P., Liu, Y., & Zhang, Y., 2020. Multiscale variability of Meiyu and its prediction: A new review. Journal of Geophysical Research: Atmospheres, 125, e2019JD031496. https://doi.org/10.1029/2019JD031496

Ding Y., Liu, Y., & Hu, Z., 2021. The Record-breaking Meiyu in 2020 and associated atmospheric circulation and tropical SST anomalies. Advances in Atmospheric Sciences. https://doi.org/10.1007/s00376-021-0361-2

Hus P-C, Li T., 2012. Role of the boundary layer moisture asymmetry in causing the eastward propagation of the Madden-Julian oscillation. J Clim 25:4914–4931

Hus P-C, Lee J-Y, Ha K-J., 2016. Influence of boreal summer intraseasonal oscillation on rainfall extremes in southern China. Int J Climatol 36:1403-1412

Jiang X., T. Li, and B. Wang, 2004. Structures and mechanisms of the northward propagating boreal summer intraseasonal oscillation. J. Climate, 17, 1022-1039.

Kalnay E., M. Kanamitsu, R. Kistler, et al., 1996. The NCEP/NCAR 40-year reanalysis project. *Bull. Amer. Meteor. Soc.*, **77**:437-471

Kemball-Cook, S., B. Wang, and X. Fu, 2002. Simulation of the Intraseasonal Oscillation in the ECHAM-4 model: The impact of coupling with an ocean model. J. Atmos. Sci., 59, 1433-1453

Lau K.-M., G. Yang, and S. Shen, 1988. Seasonal and intraseasonal climatology of summer monsoon rainfall over East Asia. Mon. Wea. Rev., 116, 18-37

Li C., R. Lu, N. Dunstone, A. Scaife, P. Bett, F. Zheng, 2021a. The seasonal prediction of the exceptional Yangtze River rainfall in summer 2020, Advances in Atmospheric Sciences, 10.1007/s00376-021-1092-0

Li L., C. Zhu, R. Zhang, and B. Liu, 2021b. Roles of the Tibetan Plateau vortices in the record Meiyu rainfall in 2020. Atmos. Sci. Lett., 22, e1017. https://doi.org/10.1002/asl.1017

Li T., B. Wang, B. Wu, et al., 2017. Theories on formation of an anomalous anticyclone in western North Pacific during El Niño: A review. J. Meteor. Res., 31(6), 987–1006, doi: 10.1007/s13351-017-7147-6

Liu B., Yan, Y., Zhu, C., Ma, S., & Li, J., 2020a. Record-breaking Meiyu rainfall around the Yangtze River in 2020 regulated by the subseasonal phase transition of the North Atlantic Oscillation. Geophysical Research Letters, 47(22), 2020GL090342. https://doi.org/10.1029/2020GL090342

Liu F., Y. Ouyang, B. Wang, J. Yang, J. Ling and P. Hsu, 2020b. Seasonal evolution of the intraseasonal variability of China summer precipitation. Clim Dyn, https://doi.org/10.1007/s00382-020-05251-0

Maloney E. D., 2009. The moist static energy budget of a composite tropical intraseasonal oscillation in a climate model. J. Climate, 22, 711-729

Mao J., Wu G., 2006. Intraseasonal variations of the Yangtze rainfall and its related atmospheric circulation features during the 1991 summer. Clim Dyn 27, 815–830

Mao J., Sun Z., Wu G., 2010. 20-50-day oscillation of summer Yangtze rainfall in response to intraseasonal variations in the subtropical high over the western North Pacific and South China Sea. Clim Dyn 34, 747–761

Pan X., T. Li, Y. Sun, Z. Zhu, 2021. Cause of extreme heavy and persistent rainfall over Yangtze River in summer 2020. Adv. Atmos. Sci., https://doi.org/10.1007/s00376-021-0433-3

Qi Y., R. Zhang, T. Li and M. Wen, 2008. Interactions between the summer mean monsoon and the intraseasonal oscillation in the Indian monsoon region. Geophys Res Lett 35:L17704. https://doi.org/10.1029/2008GL034517

Qi Y., R. Zhang, and T. Li, 2016, Structure and evolution characteristics of atmospheric intraseasonal oscillation and its impact on the summer rainfall over the Yangtze River basin in 1998. Chinese J. Atmos. Sci. (in Chinese), 40, 451-462

Qi Y., T. Li, R. Zhang and Y. Chen, 2019. Interannual relationship between intensity of rainfall intraseasonal oscillation and summer-mean rainfall over Yangtze River Basin in eastern China. Clim Dyn 53, 3089-3108

Qiao S., Chen, D., Wang, B., Cheung, H.-N., Liu, F., Cheng, J., et al., 2021. The longest 2020 Meiyu season over the past 60 years: Subseasonal perspective and its predictions. Geophys Res Lett, 48, e2021GL093596. https://doi.org/10.1029/2021GL093596

Rong X. Y., R. Zhang, T. Li, and J. Z. Su, 2011: Upscale feedback of high-frequency winds to ENSO. Quart. J. Roy. Meteor. Soc., **137**(657), 894–907

Rosen R. D., D. A. Salstein and J. P. Peixoto, 1979. Variability in the annual fields of large-scale atmospheric water vapor transport. Mon. Wea. Rev., 107, 26-37

Rui H., and B. Wang, 1990. Development characteristics and dynamic structure of tropical intraseasonal convection anomalies. J. Atmos. Sci., 47, 357-379

Salstein D. A., R. D. Rosen and J. P. Peixoto, 1980. Hemispheric water vapor flux variability – streamfunction and potential fields. Atmospheric Water Vapor, A.

Deepak, T. D. Wilkerson and L. H. Ruhnke Eds., Academic Press, 1980, 557-574

Shen Y. and Xiong A., 2106. Validation and comparison of a new gauge-based precipitation analysis over mainland China. Int. J. Climatol., 36, 252-265

Takaya Y., Ishikawa, I., Kobayashi, C., Endo, H., & Ose, T., 2020. Enhanced Meiyu-Baiu rainfall in early summer 2020: Aftermath of the 2019 super IOD event. Geophys Res Lett, 47(22), e2020GL090671. https://doi.org/10.1029/2020GL090671

Tao S. and J. Wei, 2006. The westward, northward advance of the subtropical high over the west Pacific in summer. J. Appl. Meteor. Sci. (in Chinese), 17(5), 513-525.

Teng H., and B. Wang, 2003. Interannual variations of the boreal summer intraseasonal oscillation in the Asian-Pacific region. J. Climate, 16, 3572-3584.

Torrence C., and G. P. Compo, 1998. A practical guide to wavelet analysis, Bull. Am. Meteorol. Soc., 79, 61-78.

Wang B., and Z. Fan, 1999, Choice of South Asian summer monsoon indices. Bull. Amer. Meteor. Soc., 80, 629–638

Wang B., R. G. Wu, and X. H. Fu, 2000. Pacific–East Asian teleconnection: How does ENSO affect East Asian climate? J.Climate, 13, 1517–1536

Wang C. 2019. Three-ocean interactions and climate variability: A review and perspective. Clim Dyn, 53: 5119–5136, doi: 10.1007/s00382-019-04930-x

Wu B., T. J. Zhou, and T. Li, 2009. Seasonally evolving dominant interannual variability modes of East Asian climate. J.Climate, 22, 2992–3005

Xie S.-P., K. M. Hu, J. Hafner, et al., 2009. Indian Ocean capacitor effect on Indo–western Pacific climate during the summer following El Niño. J. Climate, 22, 730–747

Yan X., S. Yang, T. Wang, E. Maloney, S Dong, W. Wei and S. He, 2019. Quasi-biweekly oscillation of the Asian monsoon rainfall in late summer and autumn: different types of structure and propagation. Clim Dyn 53, 6611-6628

Yanai M., S. Esbensen and J.-H. Chu, 1973. Determination of bulk properties of tropical cloud clusters from large-scale heat and moisture budgets. J. Atmos. Sci., 30, 611-627

Yang S., Wu B. and Zhang R. et al., 2013. The zonal propagating characteristics of low-frequency oscillation over the Eurasian mid-high latitude in boreal summer. Science China: Earth Sciences, 56, 1566-1575.

Zhang R., A. Sumi, and M. Kimoto, 1996. Impact of El Niño on the East Asian monsoon: A diagnostic study of the ’86/87 and ’91/92 events. J. Meteor. Soc. Japan, 74, 49–62

Zhang R., A. Sumi, and M. Kimoto, 1999. A diagnostic study of the impact of El Niño on the precipitation in China. Adv.Atmos. Sci., 16, 229–241

Zhang R., 2001. Relations of water vapor transports from Indian monsoon with those over East Asia and the summer rainfall in China. Adv. Atmos. Sci., 18, 1005–1017. doi: 10.1007/BF03403519

Zhang R., Q. Min, and J. Su, 2017: Impact of El Niño on atmospheric circulations over East Asia and rainfall in China: Role of the anomalous western North Pacific anticyclone. *Sci. China Earth Sci.*, **60**, 1124–1132,

Zhang W., Huang, Z., Jiang, F., Stuecker, M. F., Chen, G., & Jin, F., 2021. Exceptionally persistent Madden-Julian Oscillation activity contributes to the extreme 2020 East Asian summer monsoon rainfall. Geophys Res Lett, 48, e2020GL091588. https://doi.org/10.1029/2020GL091588

Zhao C., T. Li, and T. Zhou, 2013. Precursor signals and processes associated with MJO initiation over the Tropical Indian Ocean. J. Climate, 26, 291-307

Zheng J., Wang C., 2021. Influences of three oceans on record-breaking rainfall over the Yangtze River Valley in June 2020. Science China Earth Sciences, 64, https://doi.org/10.1007/s11430-020-9758-9

Zhou Z., Xie, S. P., & Zhang, R., 2021. Historic Yangtze flooding of 2020 tied to extreme Indian Ocean conditions. Proceedings of the National Academy of Sciences of the United States of America, 118(12), e2022255118. https://doi.org/10.1073/pnas.2022255118

Figure captions:

Figure 1. Distribution of (a) cumulative rainfall in June-August 2020 and (b) its anomalies (versus the climatology in 1980-2019) over China (units: mm).

Figure 2. Time-latitude cross section of daily rain rate over eastern China (105°-120°E) in 2020 (unit: mm/day). The rectangles reflect the rainfall areas in the summer season.

Figure 3. (a) 500-hPa geopotential height averaged of June-August (JJA) in 2020 (orange contours with intervals of 30 gpm) and in climatology (blue contours with intervals of 60 gpm). The shading shows temperature anomalies at 500-hPa in JJA 2020 (unit: K). (b) Anomalies of 850-hPa wind (vectors, unit: m/s) and vorticity (shading, unit: $x10^{-5}/s$), and 500-hPa geopotential height (contours, unit: gpm) in June-August 2020.

Figure 4. Standard deviation of June-August rainfall in 2020 (unit: mm/day).

Figure 5. The Morlet wavelet power spectrum of rainfall with 1-4th harmonics removed over the Yangtze River Basin in 2020. The abscissa is time. The ordinate is the period in days. The regions enclosed by the solid black contours are the areas greater than 99% confidence.

Figure 6. Time series of daily rainfall anomalies (left axis, bars) and the anomalous of 10-20-day filtered rainfall (solid line) over the Yangtze River region (114°–118°E, 28.5°–32.5°N) in summer 2020 (both units: mm/day). Thin dashed lines denote one and minus one standard deviation of the 10-20-day filtered time series. The solid black triangles represent the peak wet or peak dry phases.

Figure 7. Evolution of 10-20-day filtered composite in geopotential height (shading: gpm) and wind (vectors: m/s) at 200-hPa from day -8 to day +6. Day 0 represents the time of peak wet phase.

Figure 8. (a) Streamfunction and non-divergent field, and (b) potential and divergent field of the vertically integrated (1000-300 hPa) water vapor flux in summer (JJA) of 2020. Streamfunction and potential are indicated by contours in unit of 10^7 kg/s; non-divergent and divergent fields are indicated by vectors in unit of kg/(ms).

Figure 9. Difference of 10-20-day filtered (a) streamfunction and non-divergent component and (b) potential and divergent component of vertically integrated water vapor flux between peaks wet and dry phase. Streamfunction and potential are indicated by shadings in unit of 10^7 kg/s; non-divergent and divergent fields are indicated by vectors in unit of kg/(ms).

Figure 10. Composite vertical structures of 10-20-day filtered specific humidity (shadings, unit: g/kg) and vertical velocity (arrows, unit: 10^{-2} Pa/s) anomalies averaged between 110°E and 120°E at peak dry (a) and peak wet (b) phase.

Figure 11. Composite vertical structures of 10-20-day filtered vorticity (shadings, unit: 10^{-5}/s) and divergence (contours, unit: 10^{-6} /s) anomalies averaged between 110°E and 120°E at peak dry (a) and peak wet (b) phase.

Figure 12. Difference in individual moisture budget terms of 10-20-day filtered anomalous (a) moisture convergence (unit: 10^{-5}kg/(m^{2}s)) and (b) moisture advection (unit: 10^{-9}kg/(m^{2}s)) by calculating vertically integrated (1000-300 hPa) water vapor flux between peak wet and peak dry phase over the Yangtze River Basin during summer 2020.

Figure 13. (a) Vertically integrated (1000-700 hPa) 10-20-day filtered specific humidity and LFBS wind fields in term $(-q'\nabla \cdot \overline{\mathrm{V}})$ and (b) Vertically integrated 10-20-day filtered wind and LFBS specific humidity fields in term $(-\bar{q}\nabla \cdot V')$ averaged for the peak wet phases. Blank areas in (a) and (b) denote the Tibetan Plateau. Shadings denote the specific humidity in unit of g/kg and vectors denote moisture convergence in unit of 10^{-5}kg/(m^{2}s).

Figure 14. Composite vertical profiles of 10-20-day filtered (a) advection of temperature (unit: 10^{-5} ℃ /s), (b) vertical pressure velocity (unit: Pa/s), (c) wind divergence (unit: 10^{-5}/s) and (d) specific humidity (unit: g/kg) for peak wet (blue) and dry (red) phase averaged over the YRB.

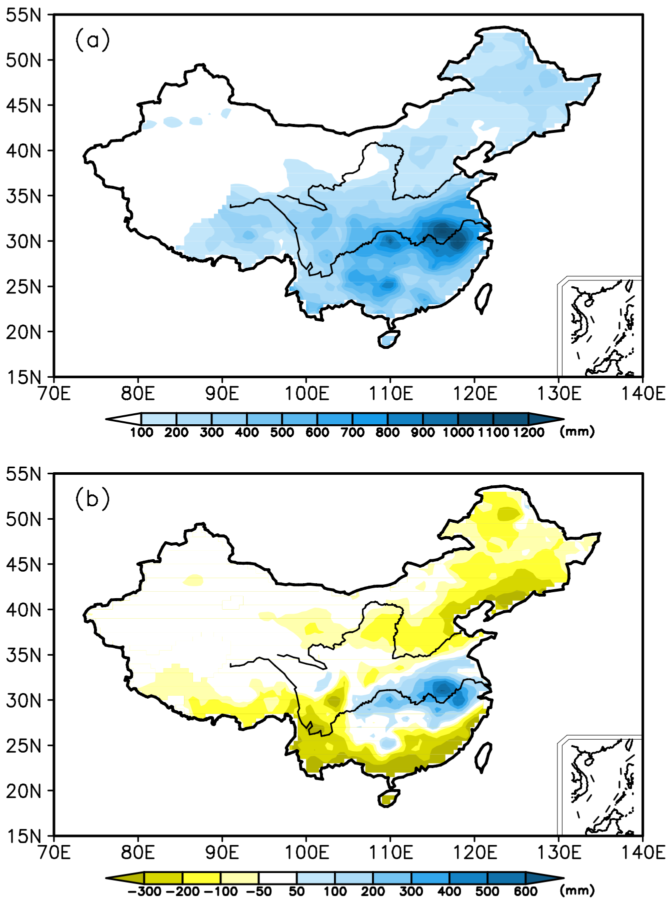

Fig.1 Distribution of (a) cumulative rainfall in June-August 2020 and (b) its anomalies (versus the climatology in 1980-2019) over China (units: mm).

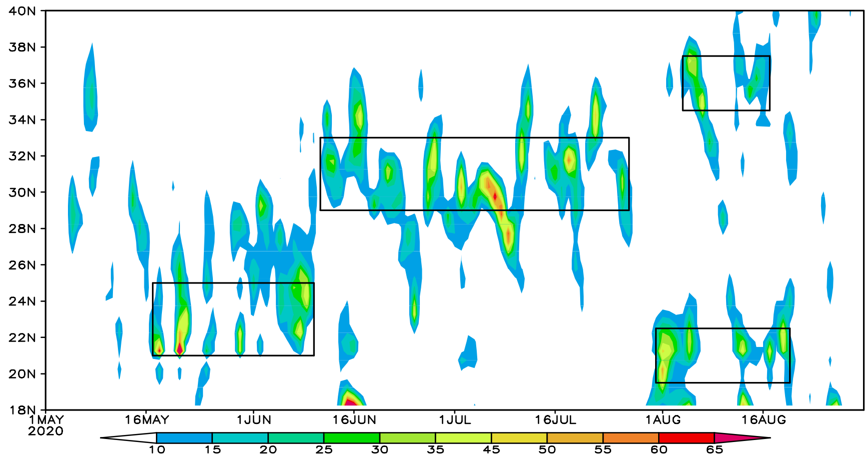

Fig.2 Time-latitude cross section of daily rain rate over eastern China (105°-120°E) in 2020 (unit: mm/day). The rectangles reflect the rainfall areas in the summer season.

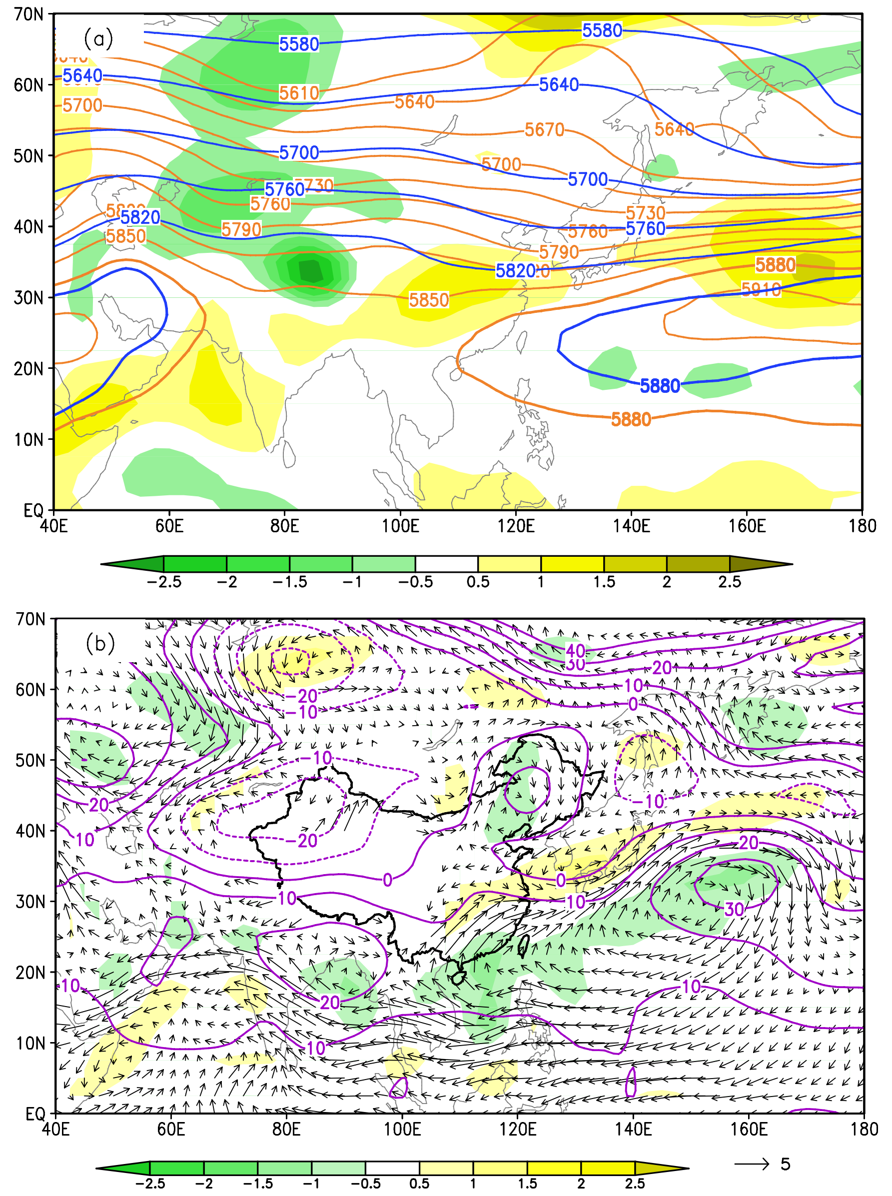

Fig.3 (a) 500-hPa geopotential height averaged of June-August (JJA) in 2020 (orange contours with intervals of 30 gpm) and in climatology (blue contours with intervals of 60 gpm). The shading shows temperature anomalies at 500-hPa in JJA 2020 (unit: K). (b) Anomalies of 850-hPa wind (vectors, unit: m/s) and vorticity (shading, unit: x10^{-5}/s), and 500-hPa geopotential height (contours, unit: gpm) in June-August 2020.

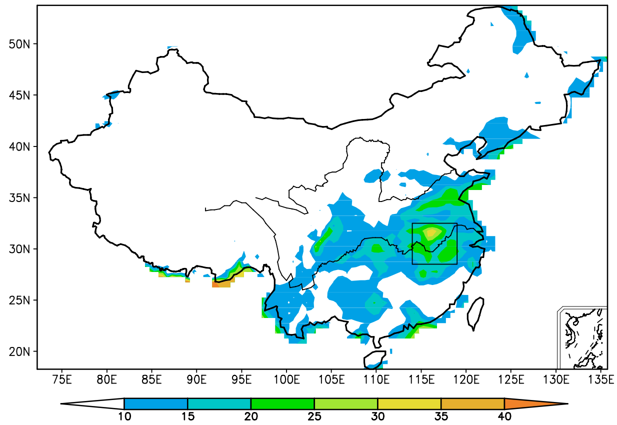

Fig.4 Standard deviation of June-August rainfall in 2020 (unit: mm/day).

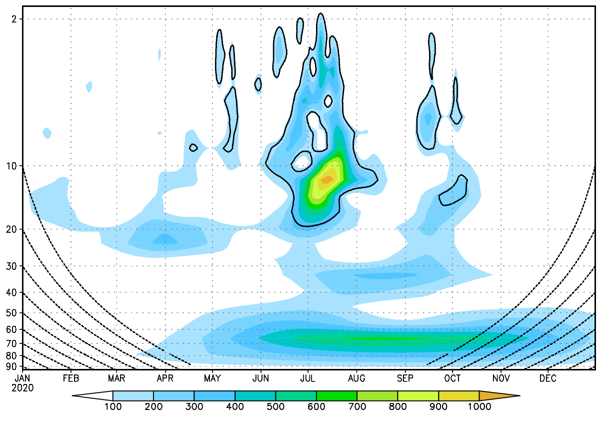

Fig.5 The Morlet wavelet power spectrum of rainfall with 1-4th harmonics removed over the Yangtze River Basin in 2020. The abscissa is time. The ordinate is the period in days. The regions enclosed by the solid black contours are the areas greater than 99% confidence.

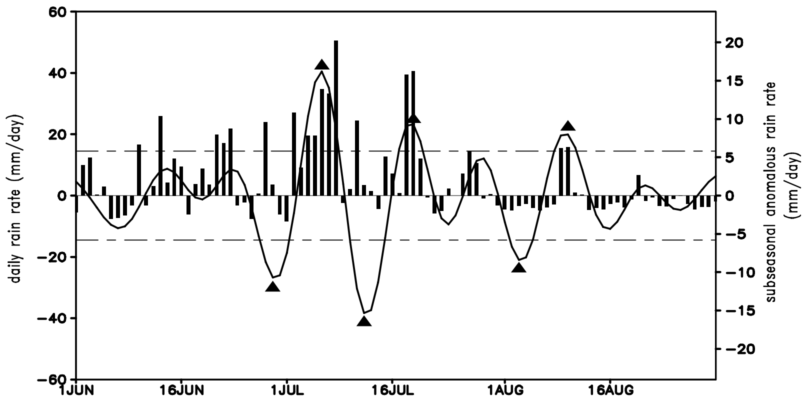

Fig.6 Time series of daily rainfall anomalies (left axis, bars) and the anomalous of 10-20-day filtered rainfall (solid line) over the Yangtze River region (114°–118°E, 28.5°–32.5°N) in summer 2020 (both units: mm/day). Thin dashed lines denote one and minus one standard deviation of the 10-20-day filtered time series. The solid black triangles represent the peak wet or peak dry phases.

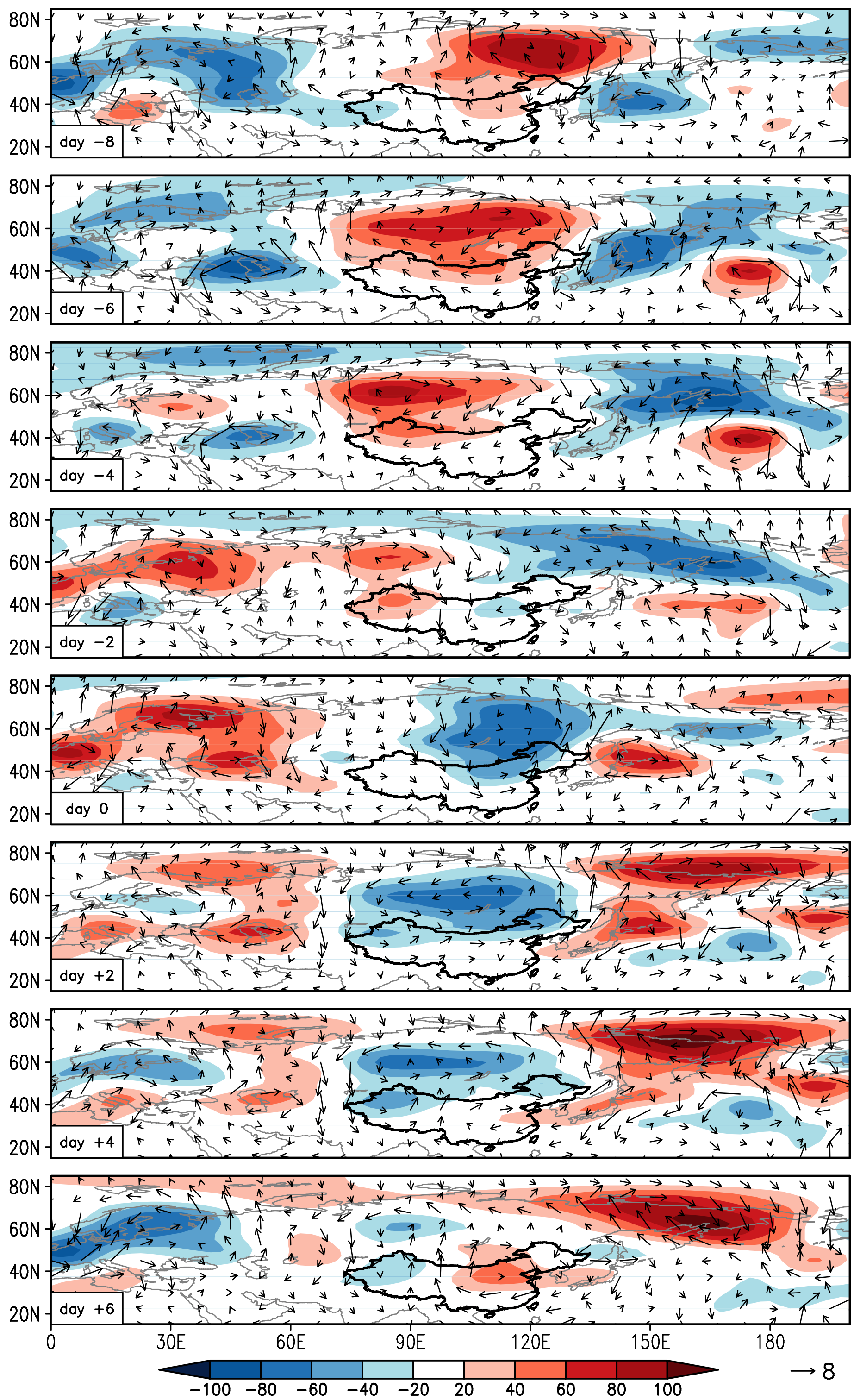

Fig.7 Evolution of 10-20-day filtered composite in geopotential height (shading: gpm) and wind (vectors: m/s) at 200-hPa from day -8 to day +6. Day 0 represents the time of peak wet phase.

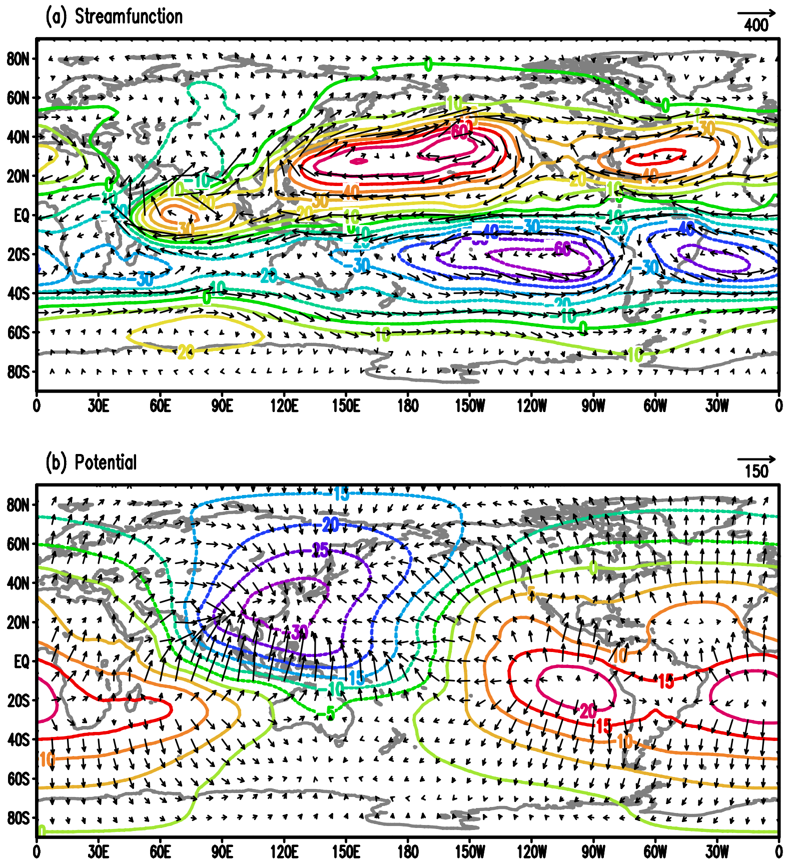

Fig.8 (a) Streamfunction and non-divergent field, and (b) potential and divergent field of the vertically integrated (1000-300 hPa) water vapor flux in summer (JJA) of 2020. Streamfunction and potential are indicated by contours in unit of 10^7 kg/s; non-divergent and divergent fields are indicated by vectors in unit of kg/(ms).

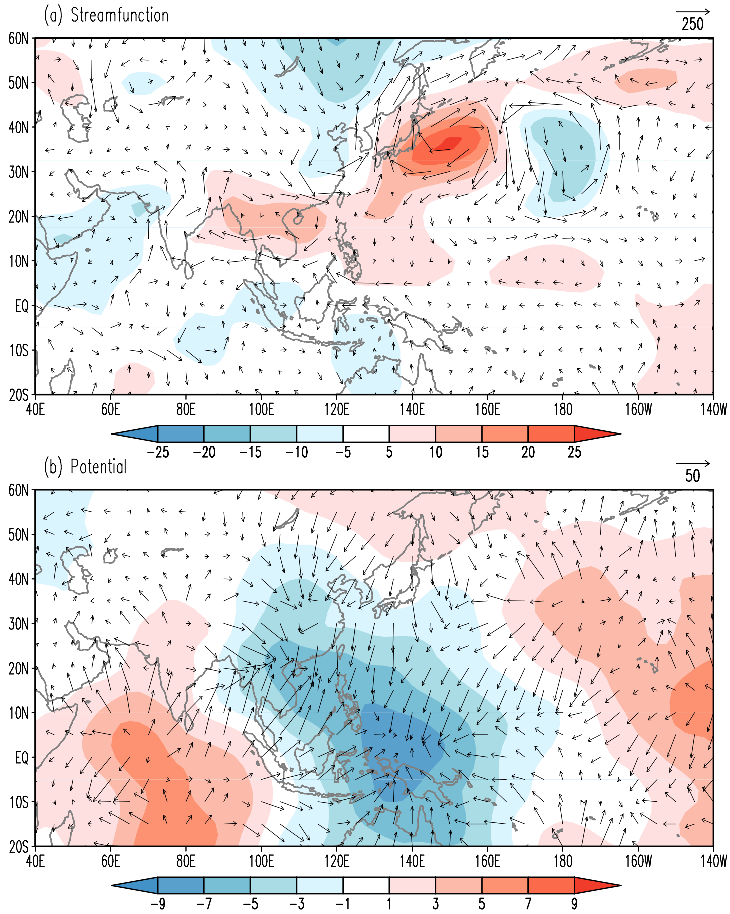

Fig.9 Difference of 10-20-day filtered (a) streamfunction and non-divergent component and (b) potential and divergent component of vertically integrated water vapor flux between peaks wet and dry phase. Streamfunction and potential are indicated by shadings in unit of 10^7 kg/s; non-divergent and divergent fields are indicated by vectors in unit of kg/(ms).

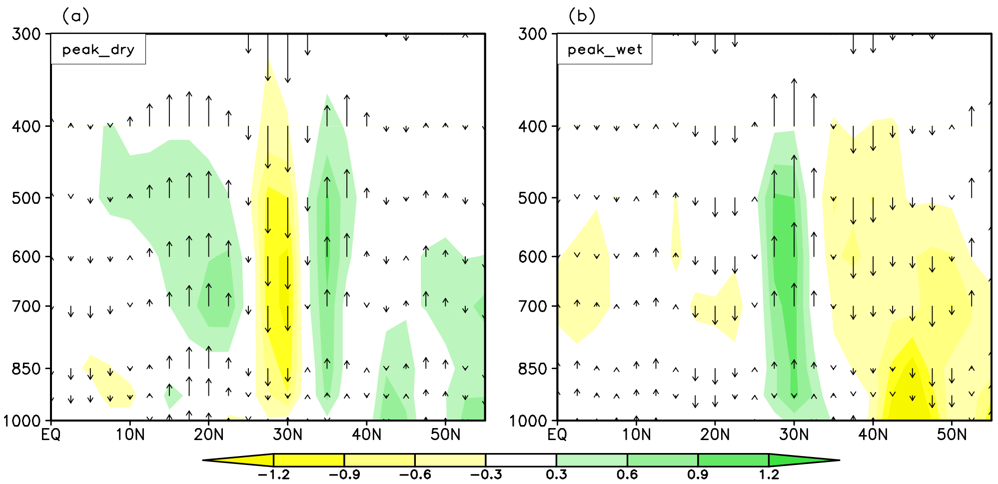

Fig.10 Composite vertical structures of 10-20-day filtered specific humidity (shadings, unit: g/kg) and vertical velocity (arrows, unit: 10^{-2} Pa/s) anomalies averaged between 110°E and 120°E at peak dry (a) and peak wet (b) phase.

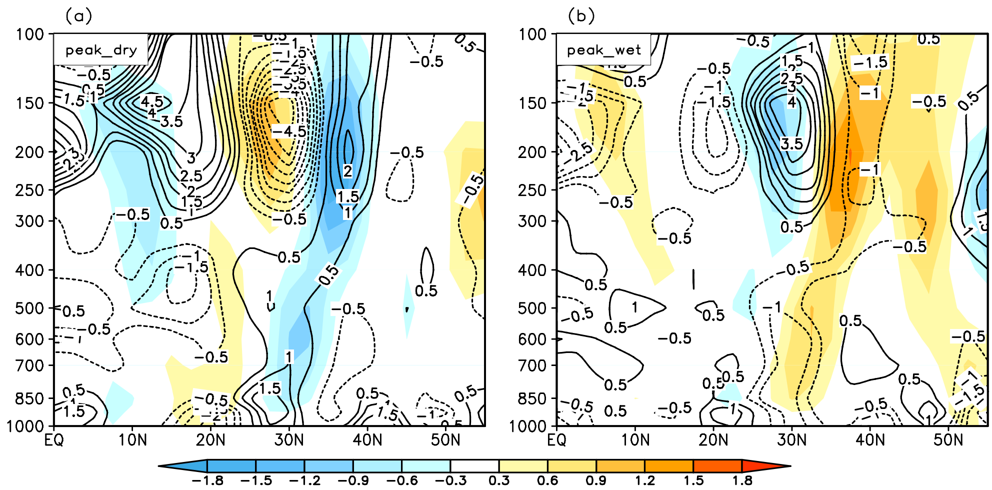

Fig.11 Composite vertical structures of 10-20-day filtered vorticity (shadings, unit: 10^{-5}/s) and divergence (contours, unit: 10^{-6} /s) anomalies averaged between 110°E and 120°E at peak dry (a) and peak wet (b) phase.

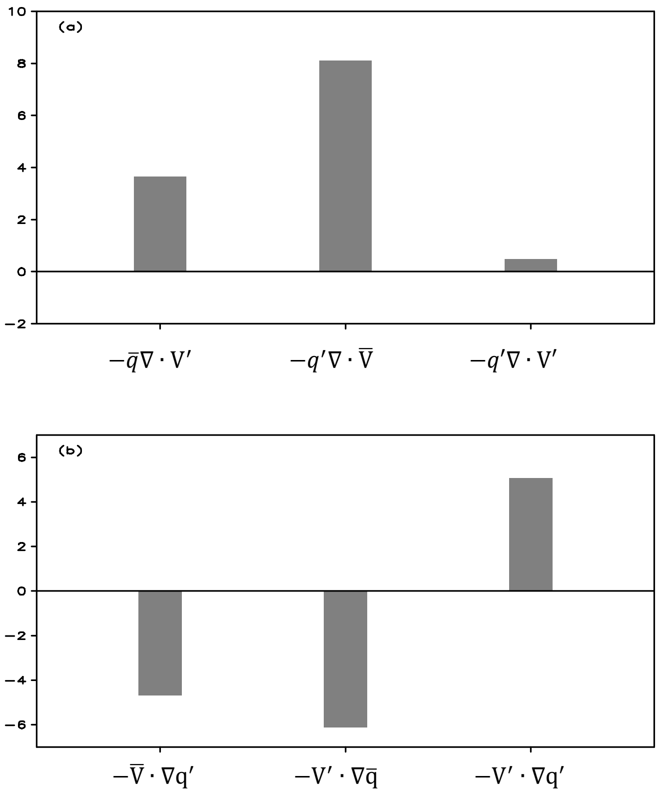

Fig.12 Difference in individual moisture budget terms of 10-20-day filtered anomalous (a) moisture convergence (unit: 10^{-5}kg/(m^{2}s)) and (b) moisture advection (unit: 10^{-9}kg/(m^{2}s)) by calculating vertically integrated (1000-300 hPa) water vapor flux between peak wet and peak dry phase over the Yangtze River Basin during summer 2020.

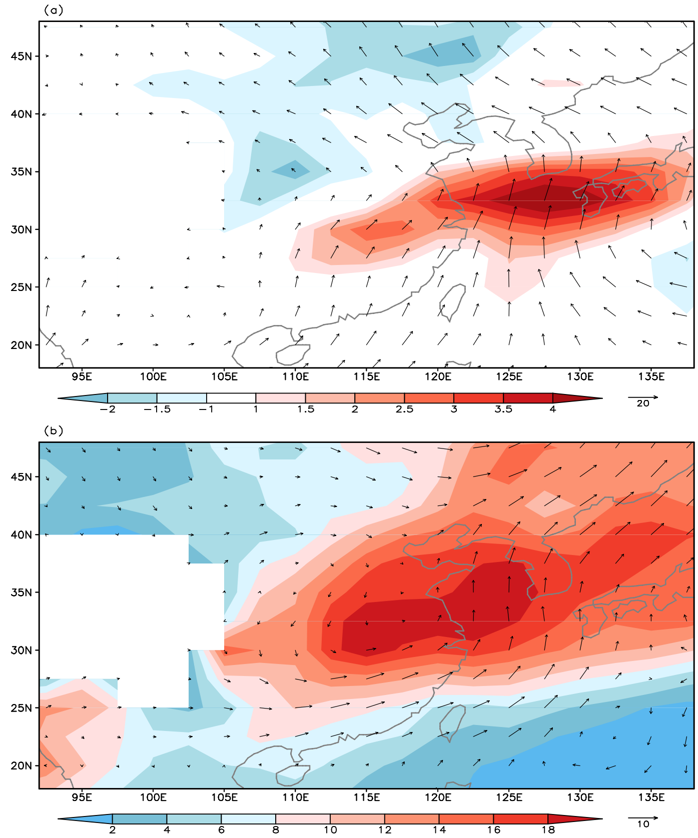

Fig.13 (a) Vertically integrated (1000-700 hPa) 10-20-day filtered specific humidity and LFBS wind fields in term $(-q'\nabla\cdot\overline{V})$ and (b) Vertically integrated 10-20-day filtered wind and LFBS specific humidity fields in term $(-\bar{q}\nabla\cdot V')$ averaged for the peak wet phases. Blank areas in (a) and (b) denote the Tibetan Plateau. Shadings denote the specific humidity in unit of g/kg and vectors denote moisture convergence in unit of 10^{-5}kg/(m^{2}s).

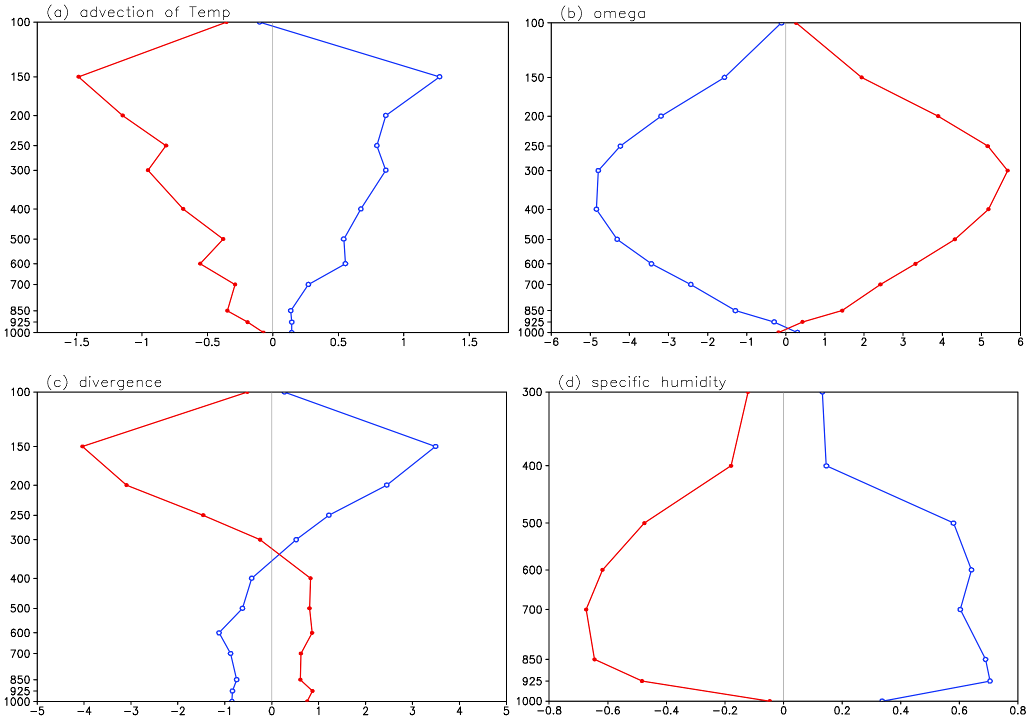

Fig.14 Composite vertical profiles of 10-20-day filtered (a) advection of temperature (unit: 10^{-5}°C/s), (b) vertical pressure velocity (unit: Pa/s), (c) wind divergence (unit: 10^{-5}/s) and (d) specific humidity (unit: g/kg) for peak wet (blue) and dry (red) phase averaged over the YRB.